



HAL
open science

Versatile Roles of Metal Species in Carbon Nanotube Templates for the Synthesis of Metal–Zeolite Nanocomposite Catalysts

Camila Flores, Vladimir L Zholobenko, Bang Gu, Nuno Batalha, Valentin Valtchev, Walid Baaziz, Ovidiu Ersen, Nilson R Marcilio, Vitaly Ordonsky, Andrei y Khodakov

► **To cite this version:**

Camila Flores, Vladimir L Zholobenko, Bang Gu, Nuno Batalha, Valentin Valtchev, et al.. Versatile Roles of Metal Species in Carbon Nanotube Templates for the Synthesis of Metal–Zeolite Nanocomposite Catalysts. *ACS Applied Nano Materials*, 2019, 2 (7), pp.4507-4517. 10.1021/acsanm.9b00888 . hal-03039965

HAL Id: hal-03039965

<https://normandie-univ.hal.science/hal-03039965>

Submitted on 4 Dec 2020

HAL is a multi-disciplinary open access archive for the deposit and dissemination of scientific research documents, whether they are published or not. The documents may come from teaching and research institutions in France or abroad, or from public or private research centers.

L'archive ouverte pluridisciplinaire **HAL**, est destinée au dépôt et à la diffusion de documents scientifiques de niveau recherche, publiés ou non, émanant des établissements d'enseignement et de recherche français ou étrangers, des laboratoires publics ou privés.

June 22nd, 2019

Versatile Roles of Metal Species in Carbon Nanotube Templates for the Synthesis of Metal-Zeolite Nanocomposite Catalysts

Camila Flores^{a, b}, Vladimir L. Zholobenko^c, Bang Gu^a, Nuno Batalha^a, Valentin Valtchev^d, Walid Baaziz^e, Ovidiu Ersen^e, Nilson R. Marcilio^b, Vitaly V. Ordonsky^{a} and Andrei Y. Khodakov^{a*}*

^a Université de Lille, CNRS, Centrale Lille, ENSCL, Univ. Artois, UMR 8181 - UCCS - Unité de Catalyse et Chimie du Solide, F-59000 Lille, France

^b Department of Chemical Engineering, Federal University of Rio Grande do Sul – UFRGS, Rua Luiz Englert, s/nº, 90040-040, Porto Alegre/RS, Brazil

^c School of Physical and Chemical Sciences, Keele University, Staffordshire, ST5 5BG, United Kingdom

^d Laboratoire Catalyse et Spectrochimie, ENSICAEN, 6 Boulevard Maréchal Juin 14050 Caen, France

^e IPCMS, Université de Strasbourg, 23, rue du Loess BP 43, F-67034 Strasbourg, France

*corresponding authors: vitaly.ordonsky@univ-lille.fr; andrei.khodakov@univ-lille.fr

Abstract

Metal-zeolite nanocomposites are extensively used in heterogeneous catalysis. The small size of zeolite micropores and non-uniform distribution of the metal component within the zeolite structure can severely reduce the efficiency of these catalysts. In this work, we propose a new single-pot synthesis strategy for the design of metal-zeolite nanocomposites with specific shape, enhanced mesoporosity and uniform distribution of highly dispersed metals such as cobalt, nickel, and magnesium within the zeolite crystals. The strategy involves using metal carbon nanotubes as a secondary hard template. The presence of metal species in carbon nanotube templates is crucial and indispensable for the synthesis of metal zeolite nanocomposites. The multiple roles of the metal carbon nanotubes in the zeolite synthesis are revealed. First, they serve as a replica to create zeolites with specific fibrous morphology. Second, they fulfill the role of a mesopore former and markedly increase the zeolite secondary porosity. Finally, they act as a vehicle to uniformly introduce the metal functions inside the mesoporous zeolites. Nanocomposites prepared using metal carbon nanotubes have shown enhanced catalytic performance in Fischer-Tropsch synthesis, hydrogenation of aromatics and anisole acylation.

Keywords: nanocomposite; hard template; replicas; catalyst; promoters; metal nanoparticles; acidity

1. Introduction

Zeolites are microporous crystalline solids with a regular pore system, which have found numerous applications in industrial processes such as oil refining, organic synthesis, adsorption and separation. The zeolite crystal structure determines the size and geometry of the micropores. They are very specific for a given type of the zeolite^{1,2} and often are comparable with the size of the reacting molecules. Small and uniform pores lead to stronger interaction between the zeolite and reacting molecules, and thus, introduce geometric and electronic confinement as well as shape selectivity phenomena in catalytic reactions involving bulky molecules³. Zeolites can be tailored to specific catalytic applications by controlling their Brønsted and Lewis acidity as well as by introducing new catalytic functions, such as metal cations, clusters, metal oxides, metalorganic complexes and enzymes³.

Zeolites in their hydrogen form are considered as acid catalysts, while metal-containing zeolites can be bifunctional catalysts that exhibit complex behavior. The concentrations and intrinsic activity of the metal and acid sites, and in particular, their localization within the zeolite structure are of utmost importance for the catalyst activity, selectivity and stability^{4,5,6}. Ion exchange, impregnation, or the introduction of a metal precursor into the zeolite synthesis gel have been often used for synthesis of metal-zeolite nanocomposites, including isomorphously substituted materials^{7, 8}. In the metal-zeolite nanocomposites, metals can be present either in the form of isolated cations in the cationic sites, or in the form of tetrahedrally coordinated cations isomorphously substituting silicon or aluminum atoms in the zeolite framework, or as small metal or oxide nanoparticles localized within the zeolite micro- or mesopores. The distribution of metal component within the zeolite is of paramount importance for the resulting catalytic performance, which can be strongly affected by the distance between metal nanoparticles and acid sites, the so-called “site intimacy”⁴ and by diffusion of the intermediates during their transport from one site to another.^{9,10,11,12}

The very small pore size of zeolites (~1 nm) imposes diffusional limitations for many catalytic reactions, in particular, for those involving bulky molecules. In order to overcome these, numerous efforts have made to synthesize nano-sized zeolite crystals¹³, extra-large pore zeolites¹⁴, or mesoporous zeolites^{15, 16}, the latter are often referred to as hierarchical zeolites. The hierarchical zeolites contain, in addition to the well-defined micropore system, mesopores with the diameters in the range of 2-50 nm. Different to zeolite micropores, the size, shape and orientation of these mesopores are not directly related to the zeolite crystalline structure. The methods used for the preparation of hierarchical zeolites could be divided into two main groups. (i) Bottom-up methods, where sacrificial templates of desired size and dimensions are incorporated into the zeolite crystals during crystallization. These templates are then eliminated by combustion or extraction. (ii) Top-down methods, including post-synthesis chemical treatment of zeolite crystals leading to the extraction of aluminum or silicon atoms and partial dissolution of the zeolite framework. Note that it is usually much more difficult to maintain zeolites with good crystallinity and to generate uniform mesopores using top-down methods such as steam treatment, acid and alkaline leaching¹⁷ compared to the bottom-up strategies.

Both hard^{18,19} and soft templates^{20,21} have been utilized to synthesize hierarchical zeolites using the bottom-up approach. The hard templates usually include carbon nanoparticles, nanotubes and polymer beads, whilst various cationic surfactants, organosilanes, cationic polymers, and ionic liquids^{22,23} are considered as soft secondary templates. Both hard and soft templates could be removed by calcination. Among the hard templates, carbon nanotubes (CNT) have attracted particular attention in the literature. CNT are very versatile materials^{24,25} as their properties are strongly affected by the presence of hydrophobic or hydrophilic functional groups, metals, oxides and other dopants. As a result, the properties of hierarchical zeolites prepared using CNT as secondary templates are strongly affected by the features of

CNT and zeolite synthesis conditions. Carbon nanotubes often contain traces of metal catalysts, which are used for their synthesis. For these reasons, the literature about the use of carbon nanotubes as templates for the synthesis of hierarchical zeolites is rather contradictory.

In this work, we found that when metal impurities had been carefully removed from the synthesized carbon nanotubes, hierarchical zeolites could not be obtained using carbon nanotubes as secondary templates. Importantly, intentional addition of CNT with metal oxides to the synthesis gel, results in excellent hierarchical zeolites. This implies that the presence of metal sites in carbon nanotubes (which can be residual metal catalysts or added metal species) is crucial for using these materials for the synthesis of hierarchical zeolites. Moreover, we uncovered multiple roles of metal-CNT in the zeolite synthesis. Firstly, they strongly affect the shape of the synthesized zeolites, which seem to be replicas of CNT and show distinct fibrous morphology. Secondly, the metal-CNT act as mesopore-forming agent and strongly enhance the zeolite mesoporous volume. Finally, zeolite synthesis in the presence of metal-CNT offers an opportunity to simultaneously introduce new catalytic functions leading to bifunctional metal-zeolite nanocomposites. The introduced metals are uniformly distributed within the zeolite crystals. The presence of metal species in CNT is essential for the synthesis of hierarchical ZSM-5 zeolites with enhanced properties and catalytic performance. Indeed, only a very limited impact on zeolite porous structure was observed by using metal-free CNT as secondary hard templates. The metal-zeolite nanocomposites prepared using metal-CNT templates exhibited improved catalytic performance in Fischer-Tropsch synthesis, hydrogenation of aromatics and anisole acylation with hexanoic acid.

2. Experimental

2.1 CNT impregnation with metal precursors

Two multi-wall CNT samples (Iolitec nanomaterial, 95%) of different size, i.e. 10-20 nm and 20-40 nm, were used. The CNT were pretreated with nitric acid in order to remove all metal contaminations. This treatment also converted CNT into their hydrophilic forms. Typically, 3 g of CNT was pretreated in 210 mL of concentrated HNO₃ (68%) for 14 h under reflux. Next, the samples were filtered, washed with distilled water until pH = 7 and dried at 100 °C overnight.

Metals were added to CNT via the wet impregnation method using Co(NO₃)₂ · 6H₂O (Sigma-Aldrich) and Pt(NH₃)₄(NO₃)₂ (Sigma-Aldrich), Mg(NO₃)₂ · 6H₂O (Sigma-Aldrich) and Ni(NO₃)₂ · 6H₂O (Sigma-Aldrich) as precursors. Co-impregnation with small amounts of platinum was solely used for the preparation of cobalt catalysts. Platinum is commonly used as a promoter in the preparation of cobalt catalysts containing small metal nanoparticles in order to improve cobalt reducibility²⁶. Typically, the precursor amount for impregnation was calculated to obtain 20 wt. % of the metal in the final catalyst. The mixture was exposed to ultrasonic treatment for 30 min and dried at 80 °C. The samples were calcined at 400 °C for 4 h under nitrogen atmosphere.

After calcination in nitrogen, the hydrophilic properties of CNT were partially lost. In order to restore the CNT hydrophilicity, the samples were treated with H₂O₂. Typically, 30 mL of 1:1 H₂O₂ (Sigma-Aldrich, 35%) and distilled water mixture were added to 2.56 g of impregnated CNT, sonicated for 30 min and dried at 80 °C. The metal supported CNT catalysts are denoted as Metal/CNT_(x) (where Metal=Co, Ni or Mg) and x is the CNT diameter in nm.

2.2 Synthesis of metal-ZSM-5 nanocomposites

The ZSM-5 zeolite was synthesized by using a synthesis gel with the initial composition of 2.7NaCl:1Al₂O₃:12.5TPAOH:55.8SiO₂:7500H₂O. The synthesis of the zeolite was carried out by mixing sodium chloride (0.380 g, Janssen Chimica, P.A.), tetrapropylammonium hydroxide (3.0 g, Sigma-Aldrich, 1 M in H₂O), sodium aluminate (0.040 g, Sigma-Aldrich) and distilled water until a clear solution was obtained. Metal/CNT (0.24 g) and tetraethyl-orthosilicate (TEOS, 2.8 g, Sigma-Aldrich, 99%) were added to this solution and the resulting synthesis gel was aged for 1 h at room temperature under stirring. Next, the zeolite crystallization was performed in a Teflon-lined autoclave (40 mL) under static condition at 170 °C for 24 h. After cooling down, the solid was recovered by filtration and washed until pH=7 was achieved. The final solid was calcined at 600 °C for 4 h in air. Further details relevant to the introduction of cobalt with CNT into ZSM-5 zeolite are available elsewhere²⁷.

For comparison, the zeolite syntheses using metal-free CNT were performed under the same conditions using a similar gel composition. The resulting zeolites were then impregnated using incipient wetness method with cobalt, nickel and magnesium nitrates as precursors.

In order to obtain the zeolite acid form, two successive exchanges using 2 M NH₄NO₃ aqueous solution at 80 °C for 1 h (1 g of zeolite per 50 mL of solution) were performed. The ammonium forms were converted into the protonic forms by calcination at 450 °C for 4 h in air. The synthesized samples were denoted as metal-CNT_(x)/ZSM-5 (where metal= Co, Ni or Mg) for the samples synthesized using metal impregnated CNT (x represents the CNT diameter, i.e. 10-20 or 20-40 nm) and CNT_(x)/ZSM-5 for the samples synthesized with pure CNT as secondary templates. Metal/ZSM-5 stands for the zeolite synthesized without any secondary template and conventionally impregnated after its synthesis with a metal nitrate followed by the nitrate decomposition via calcination in air at 500°C.

2.3 Catalyst characterization

The textural properties of the samples were determined by N₂ physisorption on a Micromeritics ASAP 2000 apparatus. Prior to the analysis, the samples were degassed under vacuum (10 µmHg) at 350 °C for 4h. The total pore volume (TPV) was calculated from the amount of vapor adsorbed at a relative pressure $P/P_0 = 0.97$. The apparent sample surface area was estimated by the BET method, while the micropore volume was calculated using the deBoer t-plot method.

The samples were characterized by X-ray diffraction (XRD) utilising a D8 Advance diffractometer equipped with an energy dispersive type detector and a monochromatic CuK_α radiation source. The samples were analyzed using a step size of 0.02° with an acquisition time of 0.5 s.

The sample chemical composition was determined by X-ray fluorescence (XRF) using a M4 TORNADO (Bruker) spectrometer. This instrument was equipped with 2 anodes, a rhodium X-ray tube 50 kV/600 mA (30 W) and a tungsten X-Ray tube 50 kV/700 mA (35 W). For sample characterization, the rhodium X-ray tube with a poly-capillary lens enabling excitation of an area of 200 µm was utilised. A silicon-drift Si(Li) detector with Peltier cooling (253 K) and a resolution <145 eV at 100000 cps (Mn K_α) was used. The measurements were conducted under vacuum (20 mbar). Quantitative analysis was carried out using fundamental parameter (standardless).

The catalyst reducibility was studied using an Autochem II (Micromeritics) temperature-programmed reduction (TPR) system. The samples were reduced under a flow of 5% H₂ in argon (50 mL/min) and heated up to 800 °C at a rate of 5°C/min. The catalyst Brønsted and Lewis acidities were monitored by infrared spectroscopy (IR) with pyridine adsorption. The IR spectra were recorded using a Thermo iS10 spectrometer (DTGC detector, 64 scans at 4 cm⁻¹ resolution). The samples were pretreated under vacuum (10⁻⁵ Torr) at 450°C for 5h.

After pre-treatment, pyridine was adsorbed on the sample at 150 °C and the excess of pyridine was then removed under vacuum (10^{-5} Torr). The spectra before and after the Py adsorption were collected at ambient temperature. The amounts of Brønsted and Lewis acid sites were calculated using the intensity of bands at $\sim 1545\text{ cm}^{-1}$ and $\sim 1455\text{ cm}^{-1}$, respectively. The absorption coefficients $\epsilon(\text{B})=1.08$ for Brønsted acid sites (peak at $\sim 1545\text{ cm}^{-1}$) and $\epsilon(\text{L})=1.71\text{ cm}\ \mu\text{mol}^{-1}$ for Lewis acid sites (peaks at $\sim 1455\text{-}1445\text{ cm}^{-1}$) were used for quantification of the zeolite acid sites.

The TEM observations of the samples were obtained by using a Jeol 2100F instrument operated at 200 kV. Before the analysis, the samples were dispersed by ultrasound in ethanol for 5 min and a drop of the suspension was deposited onto a carbon membrane on a 300 mesh copper grid. The STEM-HAADF tomographic analysis was carried out on a Jeol 2100F (field emission gun) microscope operating at 200 kV by using a spot size of $1.1\ \text{\AA}$ with a current density of $0.5\ \text{pA}\ \text{\AA}^{-1}$. Selected Area Electron Diffraction (SAED) patterns were recorded using a US1000XP CCD camera with an exposure time of 2 s on circular areas of 200 nm in diameter.

2.4 Catalytic tests

Hydrogenation of aromatics: Toluene or triisopropylbenzene hydrogenations were carried out in a fixed-bed reactor. The catalyst (50 mg) was placed into the stainless-steel reactor and then activated in a H_2 gas flow ($10\text{ cm}^3/\text{min}$, atmospheric pressure) at 400 °C for 4h with a heating rate of 2 °C/min. The reactor was cooled down to 50 °C and a hydrogen flow with a pressure of 20 bar was introduced into the reactor. The temperature was increased at 1 °C/min to the required reaction temperature (250 °C). The liquid reagents (toluene or triisopropylbenzene) were injected by a PHD ULTRA 4400 pump (Harvard Apparatus) with a flow rate of 0.8 mL/h). The products were collected in a cold trap and analyzed by a gas

chromatograph (Bruker GC-450) equipped with thermal conductivity (TCD) and flame ionization (FID) detectors.

Fischer Tropsch synthesis: the experiments were performed in a fixed-bed reactor. Prior to testing, the samples were reduced in situ in a flow of pure H₂ (3 cm³/min) at 400 °C for 4 h with a heating rate of 3°C/min. Next, the reactor was cooled down to room temperature, the flow was switched to syngas (H₂/CO = 2) and the pressure adjusted to 20 bar. Nitrogen (5% relative to CO) was used as the internal standard. After achieving the desired pressure, the temperature was increased to the reaction temperature, i.e. 250 °C, at a rate of 3 °C/min. The gas space velocities were adjusted to obtain the CO conversion of 30-40% for all catalysts. The gaseous reaction products, i.e. up to C₅, were analyzed on-line using a GC equipped with FID and TCD (Varian, CP-3800). The remaining products (wax) were condensed under pressure and analyzed ex situ on a Shimadzu GC using an FID (2010-Plus-AF).

Anisole acylation: the activity of all catalysts was evaluated in the acylation reaction between anisole and hexanoic acid according to the following protocol. The catalyst (20 mg) was added to a mixture of anisole (2 g) and hexanoic acid (0.3 g) in a reflux reactor system. The reactor was heated at 180 °C for 2 h. The products were analyzed by gas chromatography.

3. Results and Discussion

The nitrogen adsorption–desorption isotherms for the catalysts prepared by impregnation and synthesized using the Metal/CNT templates are shown in **Figure 1**. The ZSM-5 sample displays a type I isotherm exhibiting a sharp uptake at low relative pressure followed by a plateau with a hardly visible hysteresis at $P/P_0 > 0.5$. This type of isotherm is usually observed for microporous materials with textural mesoporosity generated by aggregation of small zeolite crystallites. Similar isotherms have been observed for the CNT₍₁₀₋₂₀₎/ZSM-5 and CNT₍₂₀₋₄₀₎/ZSM-5 samples synthesized using metal-free CNT as secondary hard templates

(Figure 1a). **Table 1** shows that the addition of metal-free CNT₍₁₀₋₂₀₎ during the ZSM-5 zeolite synthesis results only in a slight increase in the BET surface area and pore volume. The use of CNT₍₂₀₋₄₀₎ during the ZSM-5 zeolite synthesis does not change substantially the porous characteristics of the zeolite. This suggests that CNT without metals are poor templates for synthesis of hierarchical zeolites.

Introduction of metals (Co, Mg, Ni) via conventional impregnation without using CNT as a secondary template, has only a minor effect on the zeolite porosity and specific surface area resulting in a decrease in the zeolite pore volume and specific surface area (**Table 1**). The difference between the surface area and pore volume of the parent zeolite and its counterparts containing metals may be assigned to the effect of zeolite “dilution” by metals and partial pore blocking by the metal species. Only minor changes are observed in the microporous and mesoporous zeolite volume after the impregnation with metals. In agreement with the literature, this indicates that the metal cations are preferentially located in the zeolite micropores, whereas metal oxides species are located on the external surface of ZSM-5^{6, 28}.

Remarkably, rather different isotherms and textural properties have been observed for the ZSM-5 zeolites synthesized in the presence of the Metal/CNT templates. The zeolites prepared in the presence of Co/CNT, Ni/CNT and Mg/CNT exhibit a combination of type I and IV isotherms with a significant N₂ uptake at low relative pressure and a hysteresis loop at a high relative pressure ($P/P_0 > 0.5$, **Figures 1b-d**). Adsorption of nitrogen in the range of $P/P_0 = 0.5 - 1.0$ and relevant hysteresis can be explained by mesoporosity developed in the presence of cobalt, nickel or magnesium oxides supported on CNT. Note that almost no increase in the zeolite mesoporosity has been observed when metal-free CNT₍₁₀₋₂₀₎ or CNT₍₂₀₋₄₀₎ were used as mesoporous hard templates (**Table 1**). The presence of metal species on CNT is therefore essential for the synthesis of ZSM-5 zeolite with enhanced mesoporous volume. A slight increase in the BET surface area has been observed for CoCNT₍₁₀₋₂₀₎/ZSM-5, NiCNT₍₁₀₋

$_{20}/\text{ZSM-5}$ and $\text{MgCNT}_{(10-20)}/\text{ZSM-5}$, while the BET surface area slightly decreases when using the $\text{MeCNT}_{(20-40)}$ templates. Thus, the most significant effect of using CNT containing cobalt, nickel and magnesium is the substantial increase in the mesoporous volume. The zeolite mesoporous volume increases 2.5-4 times, when using $\text{CoCNT}_{(10-20)}$ and $\text{CoCNT}_{(20-40)}$, 4.5-5 times, when using $\text{MgCNT}_{(10-20)}$ and $\text{MgCNT}_{(20-40)}$ and 2.2-3 times for $\text{NiCNT}_{(10-20)}$ and $\text{NiCNT}_{(20-40)}$ (**Table 1**). Note that the zeolite micropore volume (between 0.09-0.13 cm^3/g) is only slightly affected by CNT supported metals used as secondary templates.

Figure S1 (see **Supporting information (SI)**) displays XRD patterns of all samples included in the present study. The characteristic XRD peaks of the MFI structure are observed in all samples, regardless of the employed synthesis procedure. No broad halo peaks, which can be attributed to the amorphous phase, have been observed. Note that the presence of metals in the catalysts leads to somewhat lower intensity of the zeolite XRD patterns, which is due to the dilution of the MFI phase with the metal oxides. In the $\text{Co}/\text{ZSM-5}$, $\text{CoCNT}_{(10-20)}/\text{ZSM-5}$ or $\text{CoCNT}_{(20-40)}/\text{ZSM-5}$ samples a peak at 36.9° which is characteristic to the Co_3O_4 can be observed. The particle size of Co_3O_4 calculated using the Scherrer equation was 27-44 nm. Such large size suggests that the main fraction of cobalt oxide is located either in large mesopores or on the zeolite external surface. The $\text{Ni}/\text{ZSM-5}$ catalyst prepared using impregnation with nickel nitrate has shown a very low intensity XRD peak at 43.2° attributed to the face-centered cubic phase NiO (JCPDS card no. #47-1049). The $\text{NiCNT}_{(10-20)}/\text{ZSM-5}$ or $\text{NiCNT}_{(20-40)}/\text{ZSM-5}$ catalysts prepared using $\text{NiCNT}_{(10-20)}$ and $\text{NiCNT}_{(20-40)}$ as hard templates show no peaks characteristic of the nickel oxide phases. No XRD peaks of Mg-containing phases have been detected in either $\text{Mg}/\text{ZSM-5}$ prepared via aqueous impregnation or in $\text{MgCNT}_{(10-20)}/\text{ZSM-5}$ and $\text{MgCNT}_{(20-40)}/\text{ZSM-5}$ catalysts prepared using hydrothermal synthesis with the MgCNT hard template. The absence of XRD peaks attributed to the metal oxide phases can be explained by smaller metal oxide particle size in the Mg- and Ni-

containing samples, which are below the XRD detection limits. It should be noted that the observed difference in the metal loading must be related to the differences in solubility of the respective metal hydroxides. Indeed, the solubility product of magnesium hydroxide is ~3 orders of magnitude greater than that for nickel and cobalt hydroxides, which is in accord with the significantly lower Mg content (c.a. 2.5%) in the nanocomposite metal-zeolites.

Figure 2 shows the TEM images of the Co, Ni and Mg containing ZSM-5 catalysts prepared using metal-CNT templates. They are very different from those usually observed for the conventional ZSM-5 zeolite. The zeolite crystallites obtained in the presence of metal CNT templates exhibit a rather irregular fibrous morphology leading to the development of zeolite mesoporosity. TEM images suggest zeolite crystallization over CNT. This morphology arises from CNT partially encapsulated inside the zeolite crystals during the zeolite synthesis. The synthesized zeolite seems to be replicas of Metal/CNT. They reproduce almost exactly the shape of the secondary templates. Importantly, the presence of metal containing CNT seems indispensable for obtaining these fibrous zeolite crystallites. The TEM images for all prepared metal-zeolite catalysts also display small metal oxide nanoparticles with the diameter between 1 and 5 nm. The presence of zeolite phase in these fibrous structures was further confirmed by selected area electron diffraction (SAED). **Figure S2, SI** displays well defined diffraction patterns and clearly indicates zeolite crystalline phase in the areas containing a larger quantity of fibrous zeolite replicas of the Metal/CNT templates.

TEM images and STEM-HAADF electron tomography of the CoCNT₍₂₀₋₄₀₎/ZSM-5 sample have confirmed localization of metal oxide nanoparticles within the zeolite (**Figure 3**). Co nanoparticles have been observed as bright spots with the size in the range 2-5 nm. STEM-HAADF images and tomography video (see **Supporting information**) show that nanoparticles are located inside the pores of CoCNT₍₂₀₋₄₀₎/ZSM-zeolite. Thus, electron microscopy, electron diffraction and tomography in combination with other characterization

techniques reveal the important function of small metal oxide clusters in CNT for the formation of mesopores in zeolite crystals. Note that no significant enhancement of the zeolite mesoporosity has been observed by using metal-free CNT as secondary templates (**Table 1**). The ZSM-5 zeolite nucleation seems to occur on the metal oxide sites located on CNT producing a hierarchical material with enhanced mesoporosity. It is important to emphasize that the stability of metal oxide nanoparticles supported on CNT in the basic medium used for zeolite synthesis is essential for obtaining hierarchical zeolites with enhanced mesoporosity. The resulting zeolite replicates the fibrous shape of CNT. The mesopores are created when CNT are removed from the zeolite by calcination. A schema illustrating the formation of hierarchical zeolite during the synthesis utilizing Metal/CNT as secondary hard templates is shown in **Figure 4**.

Cobalt and nickel temperature programmed reduction (TPR) profiles are presented in **Figure S3, SI**. The reduction patterns of the cobalt zeolite catalysts are consistent with the presence of several types of cobalt species and two-step Co_3O_4 reduction to metallic cobalt. Previous reports^{6,29,30,31} suggest that Co_3O_4 is first reduced to CoO at a lower temperature, whereas CoO is reduced to metallic Co at higher temperatures (**Figure S3a**). The $\text{Co}/\text{ZSM-5}$ sample, with cobalt added by impregnation, exhibits a TPR peak at 280°C with shoulders at $150\text{-}220^\circ\text{C}$. The shoulders at $150\text{-}220^\circ\text{C}$ in the TPR profile of $\text{Co}/\text{ZSM-5}$ can be therefore attributed to the reduction of the Co_3O_4 nanoparticles to CoO , while the major TPR peak at 280°C corresponds to the reduction of CoO to metallic cobalt. Previously, we showed^{6, 28, 32} that ZSM-5 catalysts prepared by impregnation contained a large fraction of cobalt or nickel oxide nanoparticles on the zeolite outer surface. Because of a larger solvating shell, diffusion of multi-charged ions such as cobalt or nickel, inside the ZSM-5 micropores can be rather slow³³. In all catalysts prepared by impregnation, a considerable amount of divalent metal ions are present on the zeolite external surface. The $\text{CoCNT}_{(10-20)}/\text{ZSM-5}$ and $\text{CoCNT}_{(20-}$

₄₀/ZSM-5 samples exhibit two groups of TPR peaks at 150-420°C and at 600 – 800 °C. Similar to the Co/ZSM-5 zeolite, the low temperature peaks are attributed to the reduction of small Co₃O₄ nanoparticles to metallic cobalt via the intermediate formation of CoO. The shift of these peaks to higher temperature can be explained by smaller Co₃O₄ particle sizes³⁴ and their localization inside the zeolite meso- and micropores. In agreement with previous studies^{35,36}, the peaks at higher temperature are assigned to cobalt silicates or aluminates. These mixed compounds form because of the interactions between the small metal oxide nanoparticles located on CNT and the zeolite being synthesized under the hydrothermal conditions. The TPR data are consistent with the suggestions that cobalt species supported on CNT act as nucleation sites in the synthesis of the hierarchical ZSM-5 zeolite.

The reduction profiles of the nickel catalysts prepared by impregnation with nickel nitrate and synthesized using Ni/CNT as secondary templates are shown in **Figure S3b, SI**. They exhibit broad hydrogen consumption peaks in the temperature range from 350 to 750°C. A single hydrogen consumption peak at about 400°C^{37, 38} is usually observed in the TPR profiles of bulk NiO. It corresponds to the reduction of NiO to metallic nickel. Thus, the low temperature peaks observed between 400 and 500 °C in the TPR profiles of nickel-zeolite catalysts may correspond to the reduction of small NiO particles. Note that the Ni/ZSM-5 zeolite prepared by impregnation usually contains²⁸ a significant concentration of NiO on the zeolite outer surface. These NiO nanoparticles are detected in Ni/ZSM-5 by XRD (**Figure S1, SI**). Similar to cobalt zeolite nanocomposites, the shift of the TPR peaks to a higher temperature can be due to the smaller NiO particle size and some diffusional limitations during their reduction arising from the localization of these small NiO nanoparticles in the porous material³⁹. The area of the low temperature TPR peaks between 400 and 500 °C significantly decreases for the catalysts prepared using Ni/CNT as secondary templates. This corresponds to a decrease in the concentration of the NiO particles on the zeolite outer surface. The TPR profiles of the

NiCNT₍₁₀₋₂₀₎/ZSM-5 and NiCNT₍₂₀₋₄₀₎CNT/ZSM-5 catalysts exhibit low intensity peaks at 500-700°C. High temperature TPR peaks can be attributed to the reduction of highly dispersed nickel species^{39,40} or to the presence of nickel silicate (phyllosilicate) species^{38,41,42}. In agreement with other characterization methods, the TPR results clearly show that the introduction of nickel and cobalt species with CNT during the zeolite hydrothermal synthesis leads to a higher metal dispersion. In cobalt catalysts, metal nanoparticle localization within the zeolite meso- and micropores also leads to the formation of mixed compounds between the metal oxide and silica or alumina.

The acidity of metal-zeolite catalysts has been characterized by FTIR using adsorption of pyridine (Py) as a probe for Brønsted (BAS) and Lewis acid sites (LAS). The FTIR spectra recorded after Py adsorption on the reduced catalysts are displayed in **Figure 5**. The parent ZSM-5 zeolite exhibits characteristic bands at ~1545 and 1455-45 cm⁻¹ assigned to the pyridinium ion (PyH⁺) formed on BAS and to Py adsorbed on LAS (which may also include metal ions such as Co²⁺, Ni²⁺ or Mg²⁺), respectively. Py adsorbed on both the LAS and BAS also displays a band at 1490 cm⁻¹. The concentrations of BAS and LAS calculated from the intensities of the bands at ~1545 and 1455-45 cm⁻¹ are shown in **Table 1**. Impregnation of the ZSM-5 zeolite with the Co²⁺, Ni²⁺, and Mg²⁺ cations leads to a significant decrease in the concentration of BAS. The effect is more pronounced for the Mg²⁺ impregnated ZSM-5. A much lower concentration of BAS in the impregnated catalysts can be explained by the ion exchange of the protons of the zeolite bridging OH groups with the Mg²⁺, Ni²⁺ and Co²⁺ ions. Small metal oxide clusters can also block some zeolite micropores, thus making some of BAS inaccessible for Py adsorption. Interestingly, at the same metal content in the zeolites, the decrease in the concentration of BAS is less significant, when the cations are introduced with the Metal/CNT hard templates. This suggests that a significant fraction of the metal species added with Metal/CNT are probably not localized in the cationic zeolite sites but present as

small oxide clusters in the zeolite micro- and mesopores. This explains a less significant decrease in the number of BAS in the zeolites synthesized using the Metal/CNT hard templates with the same metal contents.

The number of LAS is considerably higher in all metal containing ZSM-5 as compared to their metal-free ZSM-5 counterpart (**Table 1**). The addition of the metals results in the generation of new types of LAS such as coordinatively unsaturated Co^{2+} , Ni^{2+} or Mg^{2+} cations. Some of these cations can occupy zeolite cationic sites. Interestingly, a much lower concentration of LAS is generated in the metal zeolite catalysts prepared using zeolite crystallization in the presence of metal CNT secondary templates as compared to the sample prepared by zeolite impregnation with nitrates. This can be due to a lower concentration of Co^{2+} , Ni^{2+} and Mg^{2+} in the cationic sites of the hierarchical zeolites. This also indicates the formation of metal oxide clusters and is consistent with a smaller decrease in the number of BAS in the zeolites prepared using the Metal/CNT hard templates. Overall, both metal oxide nanoparticles and ion-exchanged metal cations are formed in the synthesised metal-zeolite nanocomposite catalysts, as demonstrated by a combination of characterisation techniques. However, the number of isolated M^{2+} cations in the Metal-CNT/ZSM-5 samples is considerably lower as compared to the Metal/ZSM-5 samples prepared via “conventional” impregnation.

Catalytic Performance in Fischer-Tropsch Synthesis, Hydrogenation and Acylation Reactions

The results of catalytic tests of cobalt zeolite catalysts in Fischer-Tropsch synthesis are presented in **Table S1, SI**. Hydrocarbons and water are major reaction products of carbon monoxide hydrogenation. Extremely small amounts of CO_2 have been observed. By varying GHSV between 20 and 70 L/h g_{Co} , the CO conversion of 30-40% has been obtained for all

catalysts. The reaction rate normalized by the total amount of cobalt in the catalysts slightly increases for CoCNT₍₁₀₋₂₀₎/ZSM-5 and decreases in CoCNT₍₂₀₋₄₀₎/ZSM-5 compared to the Co/ZSM-5 sample prepared by conventional impregnation. Note however, that TPR (**Figure S3a, SI**) is indicative of very different cobalt reducibility in different samples. The addition of the Co/CNT hard templates during the zeolite synthesis results in the formation of barely reducible cobalt silicate or cobalt aluminate species, which exhibit TPR peaks at 600-800 °C. The peaks at 600-800 °C are absent in the TPR profiles of Co/ZSM-5. This suggests a low concentration of cobalt silicates or aluminates in the Co/ZSM-5 catalyst prepared by impregnation. Interestingly, the activity per reducible cobalt increased 5-10 times over CoCNT/ZSM-5 prepared using CoCNT as secondary templates in comparison with Co/ZSM-5 prepared by impregnation²⁷. The higher activity (per reducible cobalt) over CoCNT₍₁₀₋₂₀₎/ZSM-5 can be explained by enhanced mesoporosity and more uniform distribution of cobalt nanoparticles within the zeolite. The enhanced diffusion of the reagents, intermediates between metal and zeolite acid sites in combination with easy removal of the reaction products result in higher catalytic activity of the metal zeolite nanocomposites.

The methane selectivity varies between 13-33%. Previous data⁴³ suggest that the higher methane selectivity over zeolite-based catalysts can be due to more significant diffusion limitations for carbon monoxide molecules compared to hydrogen. Slower diffusion of CO relative to hydrogen results in the CO deficiency the zeolite pores. The resulting higher H₂/CO ratio in the narrow zeolite pores leads to a higher contribution of methanation reaction and higher methane selectivity. Importantly, lower methane selectivity was observed over CoCNT₍₁₀₋₂₀₎/ZSM-5 and CoCNT₍₂₀₋₄₀₎/ZSM-5 with larger mesoporous volume. These catalysts may have less significant diffusion limitations compared to mostly microporous Co/ZSM-5, where cobalt was added by impregnation. The catalysts prepared using the CoCNT₍₁₀₋₂₀₎ and CoCNT₍₂₀₋₄₀₎ hard templates also exhibit a higher selectivity to the C₅⁺

products (around 74%) as compared to the conventional Co/ZSM-5 catalysts which shows C₅₊ selectivity of 48% (**Table S1, SI**).

Nickel catalysts have been tested in the toluene and 1,3,5-triisopropylbenzene hydrogenation (**Table 2**). These reactions have been used to evaluate the activity and accessibility of nickel metal sites in the hierarchical zeolites. The mesoporosity developed in the nickel-zeolite catalysts synthesized in the presence of Ni/CNT secondary templates results in a significantly higher hydrogenation rate in both toluene and 1,3,5-triisopropylbenzene reactions. The reaction rate increases in the order: Ni/ZSM-5 < NiCNT₍₁₀₋₂₀₎/ZSM-5 < NiCNT₍₂₀₋₄₀₎/ZSM-5. This is indicative of a better nickel dispersion and enhanced accessibility of nickel metallic sites in the zeolites prepared using the Ni/CNT hard templates. Noteworthy, the zeolite prepared using NiCNT₍₂₀₋₄₀₎ with larger CNT diameter exhibited higher reaction rate in both toluene and 1,3,5-triisopropylbenzene hydrogenation reactions.

Zeolites usually contain a significant number of acid sites. Acylation of anisole with hexanoic acid has been selected as a model reaction to characterize the catalytic performance of the acid sites on the outer surface and in the mesopores of the hierarchical zeolites (**Schema, SI**). On all catalysts evaluated in the present work, the reaction results in the formation of ortho-methoxy-hexyl-phenone with the selectivity higher than 90%, while the selectivity to the para-isomer was less than 10%. Only traces of the meta-isomer have been detected. Note that the size of the ortho-isomer is much larger than the diameter of micropores in the ZSM-5 zeolite. The higher selectivity to the larger ortho-methoxy-hexyl-phenone is consistent with the critical role of the zeolite acid sites on the zeolite outer surface and mesopores in this reaction. The hexanoic acid conversion and reaction rate are shown in **Table 3**. For all the catalysts, the conversion increases when Metal/CNTs have been added as hard templates during the zeolite synthesis. The conversion increases by a factor of 2-4 over CoCNT₍₁₀₋₂₀₎/ZSM-5 and CoCNT₍₂₀₋₄₀₎/ZSM-5, 1.3-1.6 over NiCNT₍₁₀₋₂₀₎/ZSM-5 and NiCNT₍₂₀₋₄₀₎/ZSM-

5 and 4.5-5.0 over $\text{MgCNT}_{(10-20)}/\text{ZSM-5}$ and $\text{MgCNT}_{(20-40)}/\text{ZSM-5}$ in comparison with their counterparts prepared via impregnation. The effect is more pronounced when CNT had a relatively large (20-40 nm) diameter. The highest conversion has been achieved over $\text{NiCNT}_{(20-40)}/\text{ZSM-5}$. **Figure 6** shows the relation between the conversion of hexanoic acid and the number of Brønsted acid sites in the catalysts. Both the concentration of Brønsted acid sites and the presence of mesopores created in the ZSM-5 zeolite in the presence of metal supported CNT affect the catalytic performance in the anisole acylation. Interestingly, at a similar concentration of BAS, the higher acylation rates are observed for the catalysts with higher mesoporosity. Indeed, zeolites with larger mesopores obtained using Metal/CNT with the diameter of 20-40 nm are the most active in this reaction. This suggests a better accessibility of both BAS and metal sites in the hierarchical ZSM-5 prepared using the Metal/CNT templates. Hence, the strategy for the synthesis of hierarchical zeolites using metal supported CNT as secondary hard templates seems promising. It produces hierarchical zeolites replicating the shape of CNT with enhanced mesoporosity and highly dispersed, accessible and uniformly distributed metal nanoparticles and acid sites, which would be beneficial for a number of important catalytic reactions.

Conclusion

Our paper provides a new synthesis strategy for the preparation of hierarchical zeolites. It involves metal supported carbon nanotubes as secondary templates. The Metal/CNT templates play three roles in the synthesis of hierarchical zeolite. These templates are (i) a zeolite synthesis replica, (ii) a mesoporegen and (iii) a tool to introduce uniformly distributed metal species into zeolites.

The metal oxide species seem to be nucleation sites and crystallization modifiers leading to the fibrous zeolite morphology, which largely replicates the CNT. Using Metal/CNT as templates leads a several-fold increase in the zeolite mesoporous volume. The dispersed metal species, which are present as small metal oxide nanoparticles, are uniformly distributed within the crystallites of the synthesized zeolites. The concentration of Brønsted acid sites in the zeolites synthesized using Metal/CNT as secondary templates is higher than in the zeolites with the same amount of metal species prepared via impregnation.

Owing to the enhanced diffusion of the reacting species and uniform distribution of metal nanoparticles in the zeolite, the resulting materials have shown improved catalytic performance in three catalytic reactions: Fischer-Tropsch synthesis, hydrogenation of aromatics and anisole acylation.

Our data also explain the discrepancies in the literature relevant to synthesis of hierarchical zeolites using carbon nanotubes as templates. Indeed, when nickel or other metals are removed from the carbon nanotubes utilized in zeolite synthesis, hierarchical materials cannot be obtained. In contrast, intentional addition of carbon nanotubes containing metal oxides to the synthesis gel results in successful synthesis of hierarchical zeolites with enhanced mesoporosity.

Acknowledgements

The authors are grateful to Olivier Gardoll, Laurence Burylo and Joelle Thuriot for help with TPR, XRD and XRF measurements. The authors thank International Cooperation Program CAPES/COFECUB Foundation funded by CAPES – Brazilian Federal Agency for Support and Evaluation of Graduate Education within the Ministry of Education of Brazil for providing a PhD stipend for C.F. and financial support for this work. Chevreul Institute (FR

2638), Ministère de l'Enseignement Supérieur, de la Recherche et de l'Innovation, Hauts-de-France Region and FEDER are acknowledged for supporting and funding partially this work. The authors acknowledge financial support of the French National Research Agency (DirectSynBioFuel project, Ref. ANR-15-CE06-0004 and NANO4-FUT, Ref. ANR-16-CE06-0013).

Supporting Information

3D STEM-EDX animation showing that cobalt particles, introduced during hydrothermal synthesis with CNT are located with the ZSM-5 zeolites; supplementary XRD, TPR and TEM data.

Table 1. Catalyst characterization data

Sample	N ₂ adsorption				Metal content (wt %)	Acidity*	
	S _{BET} (m ² g ⁻¹)	V _{tot} (cm ³ g ⁻¹)	V _{mic} (cm ³ g ⁻¹)	V _{meso} (cm ³ g ⁻¹)		Lewis (μmolg ⁻¹)	Brønsted (μmolg ⁻¹)
ZSM-5	425	0.19	0.13	0.06	-	36	314
CNT ₍₁₀₋₂₀₎ /ZSM-5	460	0.21	0.15	0.06	-	-	-
CNT ₍₂₀₋₄₀₎ /ZSM-5	397	0.18	0.13	0.05	-	-	-
Co/ZSM-5	372	0.17	0.11	0.07	15.6	530	160
CoCNT ₍₁₀₋₂₀₎ /ZSM-5	435	0.32	0.09	0.23	7.8	180	250
CoCNT ₍₂₀₋₄₀₎ /ZSM-5	395	0.25	0.09	0.16	9.4	130	295
Mg/ZSM-5	399	0.18	0.12	0.06	1.5	284	92
MgCNT ₍₁₀₋₂₀₎ /ZSM-5	433	0.34	0.07	0.27	2.3	48	204
MgCNT ₍₂₀₋₄₀₎ /ZSM-5	410	0.35	0.05	0.30	2.1	39	141
Ni/ZSM-5	406	0.19	0.11	0.08	5.0	172	179
NiCNT ₍₁₀₋₂₀₎ /ZSM-5	444	0.29	0.12	0.17	4.5	47	267
NiCNT ₍₂₀₋₄₀₎ /ZSM-5	434	0.23	0.10	0.13	4.6	18	220

*determined by pyridine adsorption at 150°C

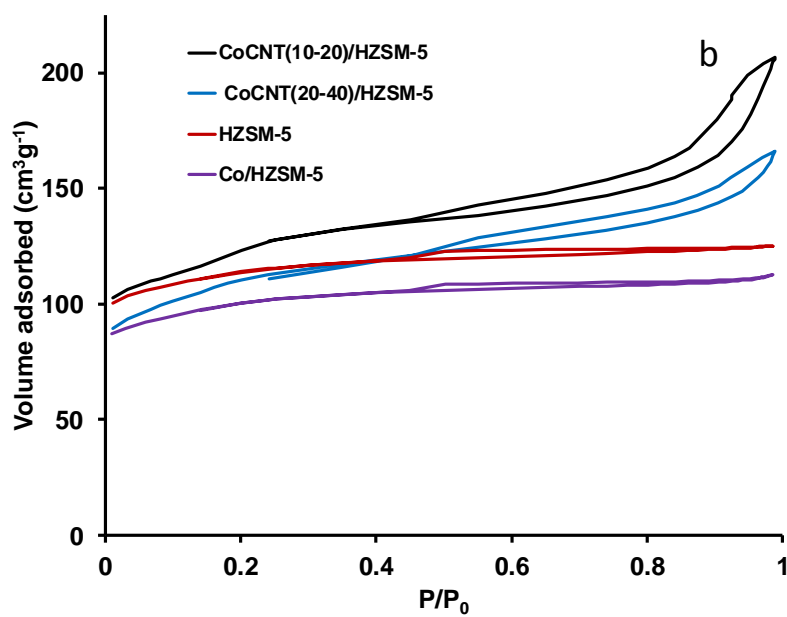
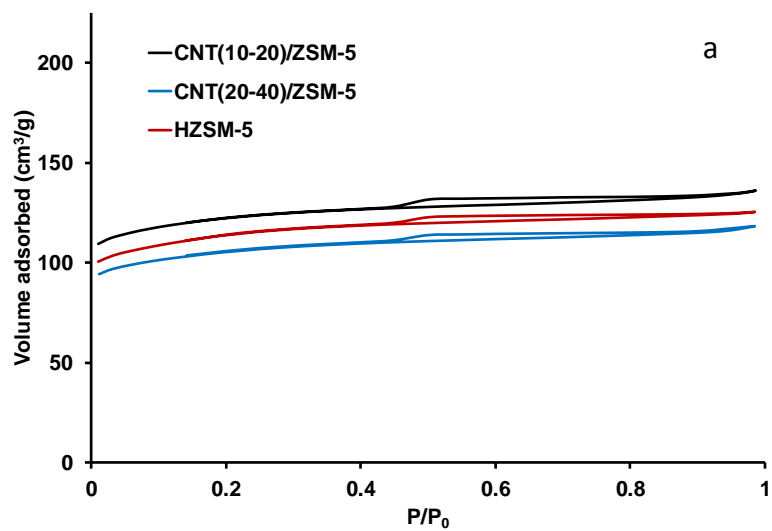
Table 2. Hydrogenation reaction ($H_2=20$ mL/min, liquid flow=0.8 mL/h, $T=250$ °C, $P=20$ bar, reaction time 6 h)

Catalyst	Toluene Conversion (%)	1,3,5- Triisopropylbenzene Conversion (%)
Ni/ZSM-5	60	23.7
NiCNT ₍₁₀₋₂₀₎ /ZSM-5	83.3	50.8
NiCNT ₍₂₀₋₄₀₎ /ZSM-5	97.7	97

Table 3. Acylation reaction (2 g of anisol, 0.3 g hexanoic acid, 20 mg of the catalyst, T=180°C; reaction time 2 h)

Catalyst	Conversion (%)	Reaction rate ($\mu\text{mol/g min}$)
Co/ZSM-5	0.43	4.63
CoCNT ₍₁₀₋₂₀₎ /ZSM-5	1.00	10.78
CoCNT ₍₂₀₋₄₀₎ /ZSM-5	1.79	19.29
Ni/ZSM-5	1.53	16.49
NiCNT ₍₁₀₋₂₀₎ /ZSM-5	1.92	20.69
NiCNT ₍₂₀₋₄₀₎ /ZSM-5	2.46	26.51
Mg/ZSM-5	0.26	2.80
MgCNT ₍₁₀₋₂₀₎ /ZSM-5	1.18	12.72
MgCNT ₍₂₀₋₄₀₎ /ZSM-5	1.31	14.12

*time at 6 h.



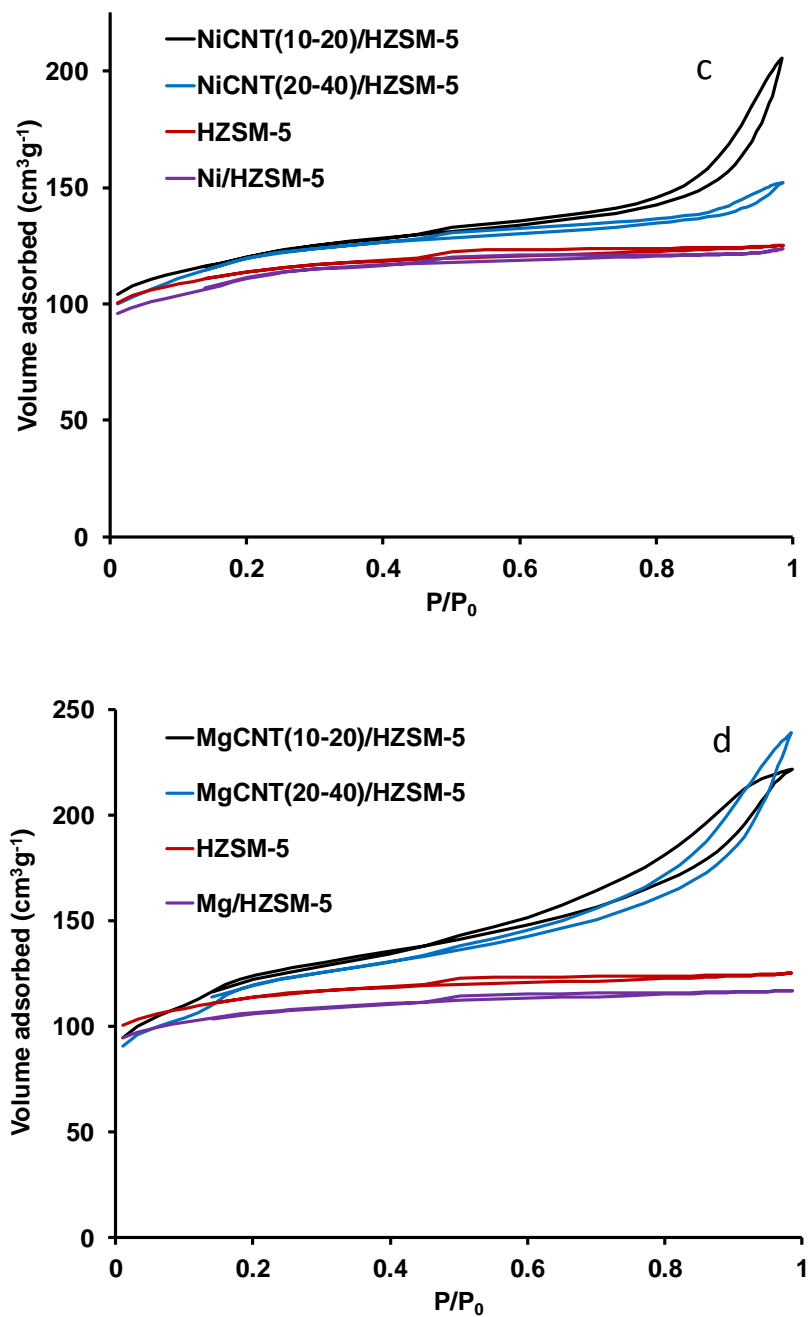


Figure 1. Low temperature nitrogen adsorption- desorption isotherms on the HZSM-5 zeolite synthesized with and without addition of CNT (a) cobalt (b), nickel (c) and magnesium (d) ZSM-5 catalysts. (The P/P_0 region below 0.01 is not shown for clarity.)

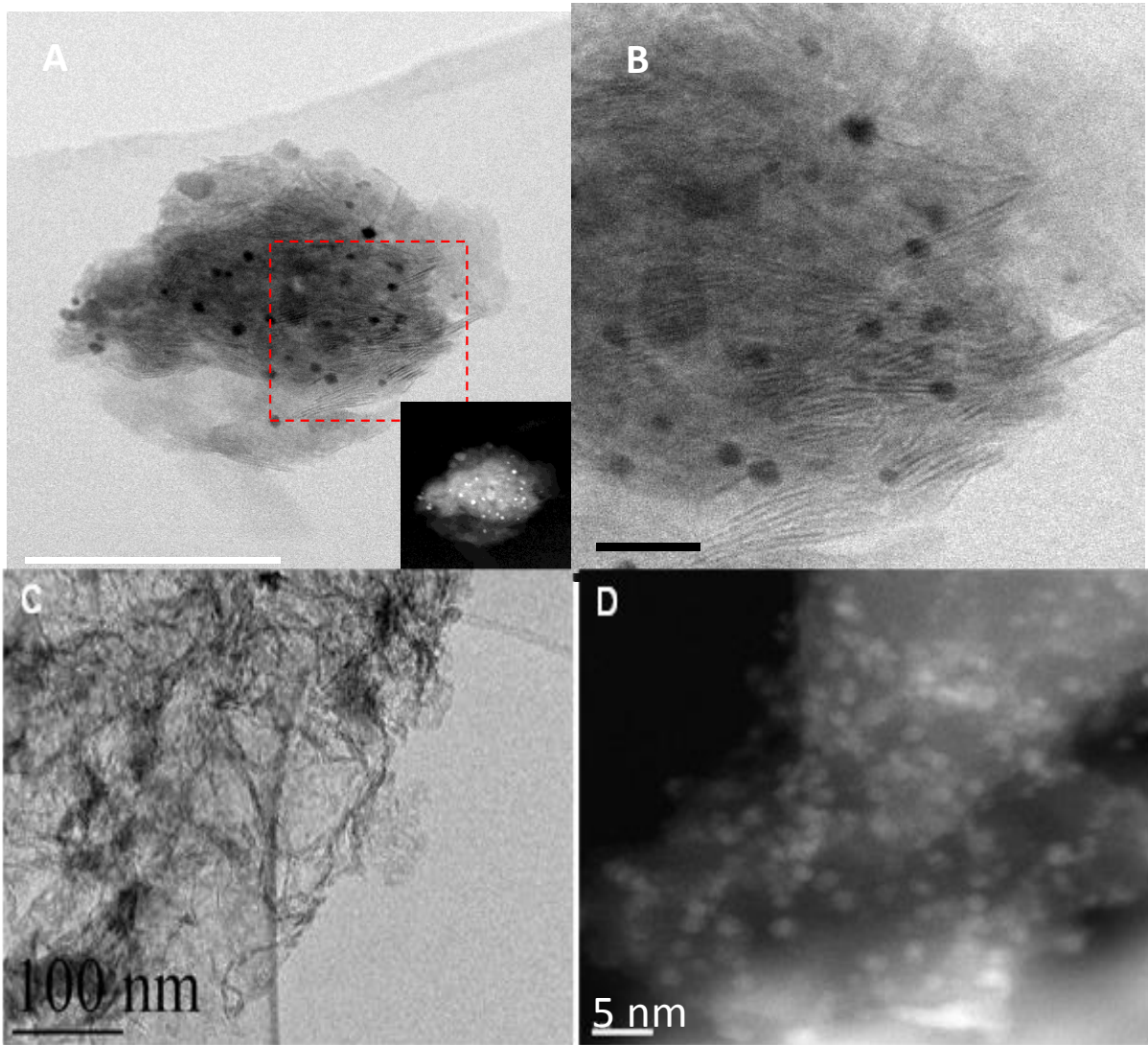


Figure 2. TEM images of CoCNT₍₁₀₋₂₀₎/ZSM-5 (A), CoCNT₍₂₀₋₄₀₎/ZSM-5 high magnification (B), MgCNT₍₁₀₋₂₀₎/ZSM-5 (C) and NiCNT₍₂₀₋₄₀₎/ZSM-5 (D).

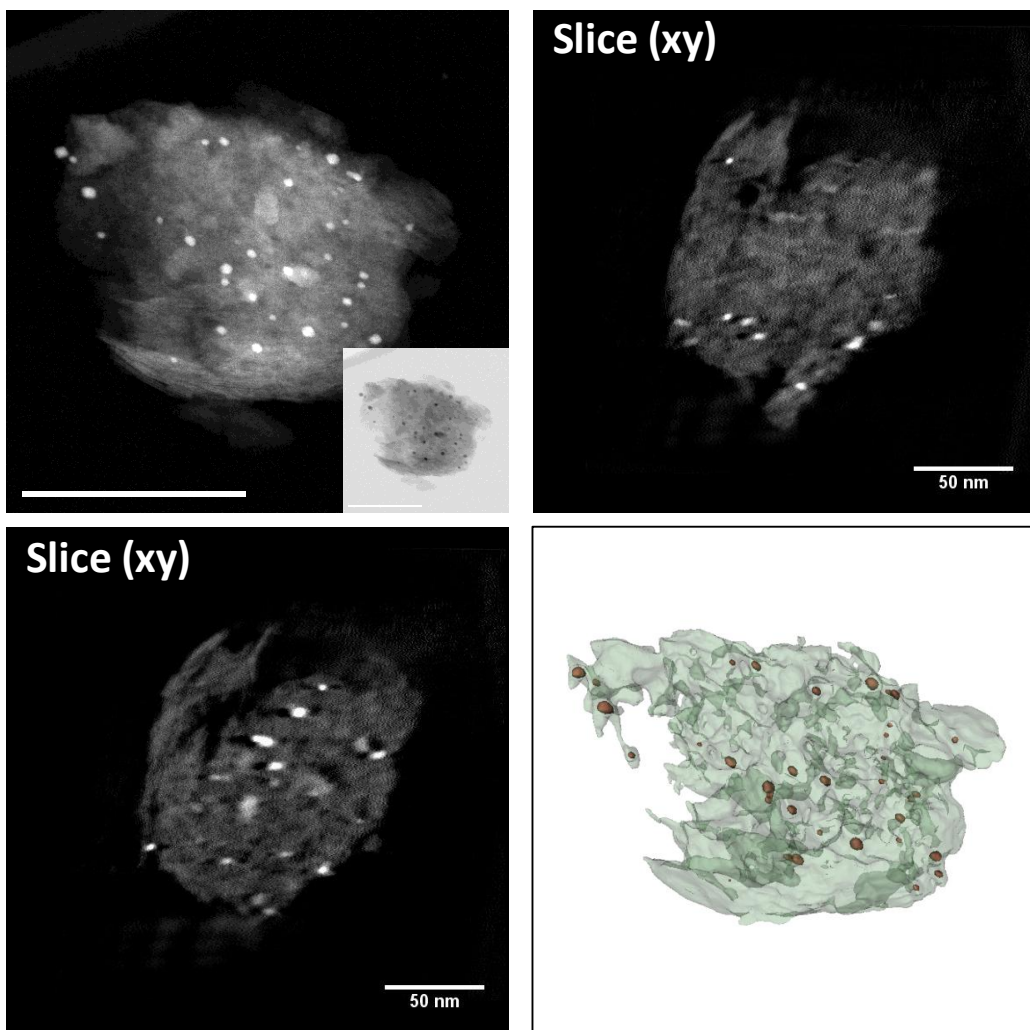


Figure 3. STEM-HAADF electron tomography analysis of CoCNT₍₂₀₋₄₀₎/ZSM-5 clearly showing the presence of cobalt nanoparticles inside the zeolite structure

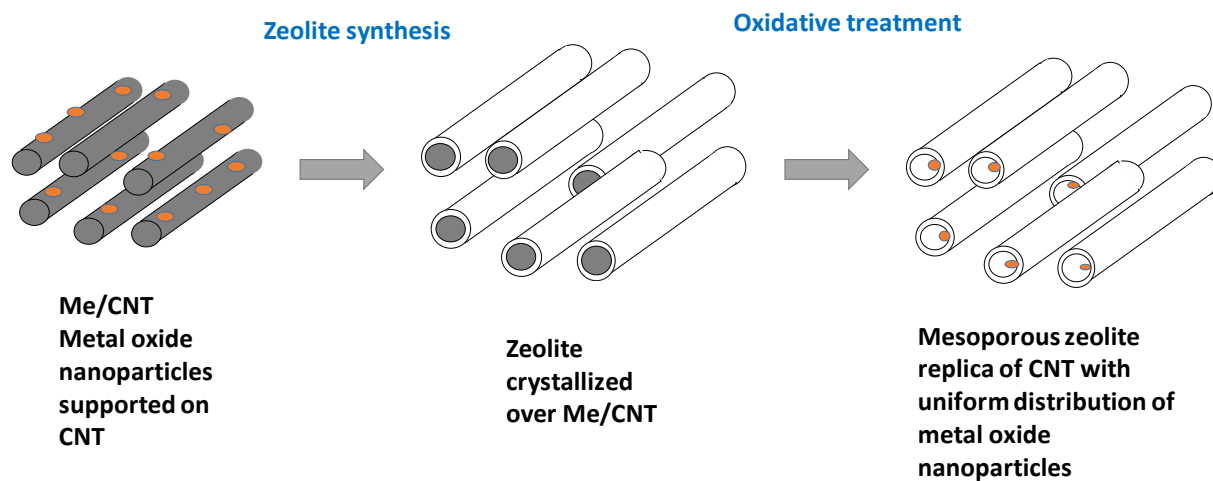
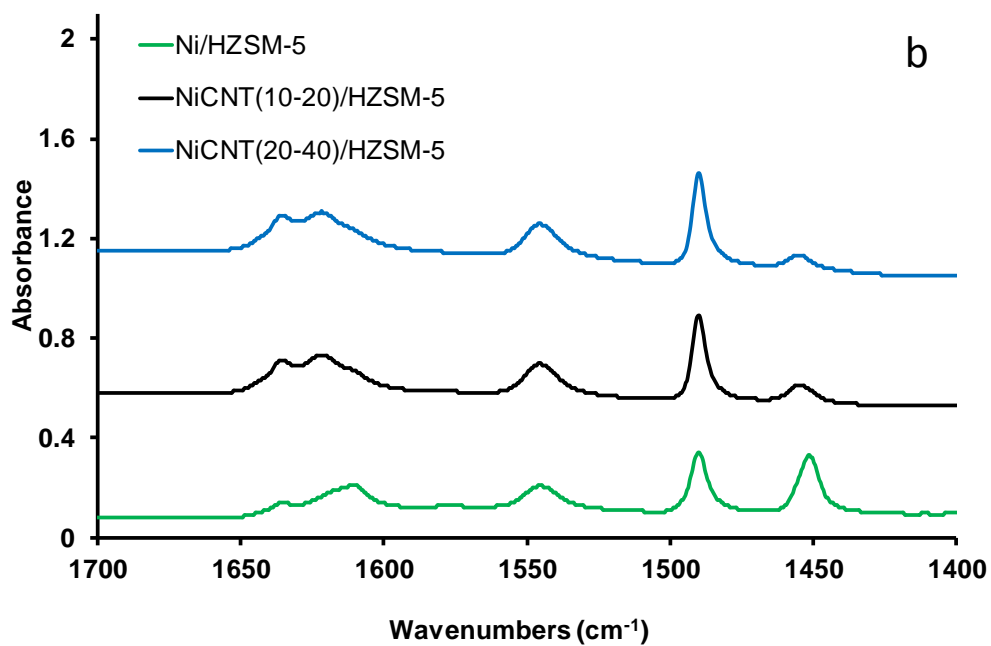
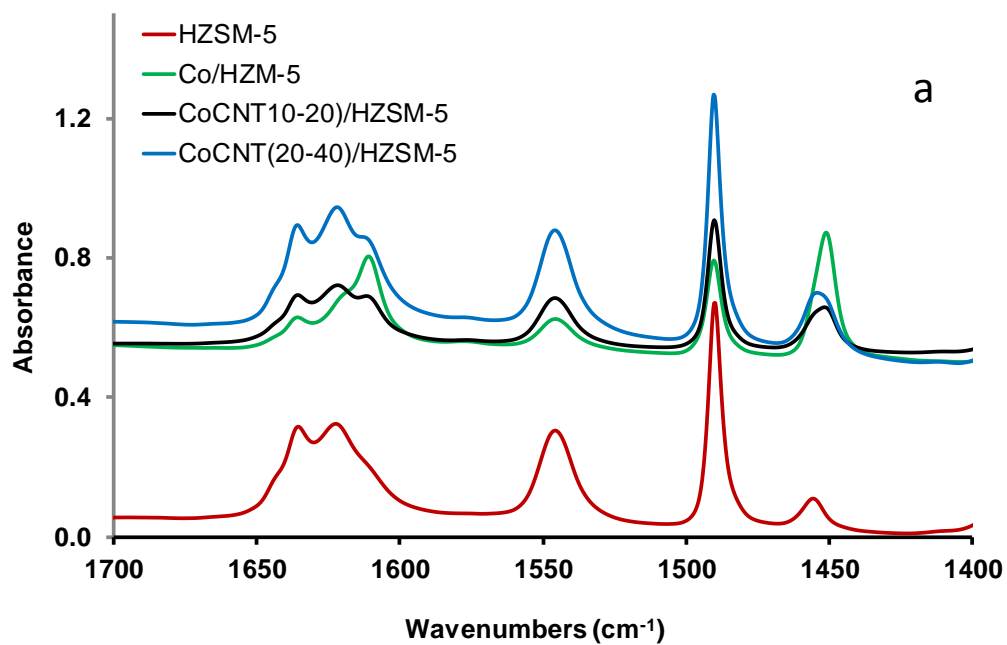


Figure 4. Synthesis of metal-zeolite nanocomposites using Metal/ CNT as secondary hard templates: simultaneous single-pot creating fibrous nanotube morphology, enhancement of mesoporosity and uniform introduction of active species



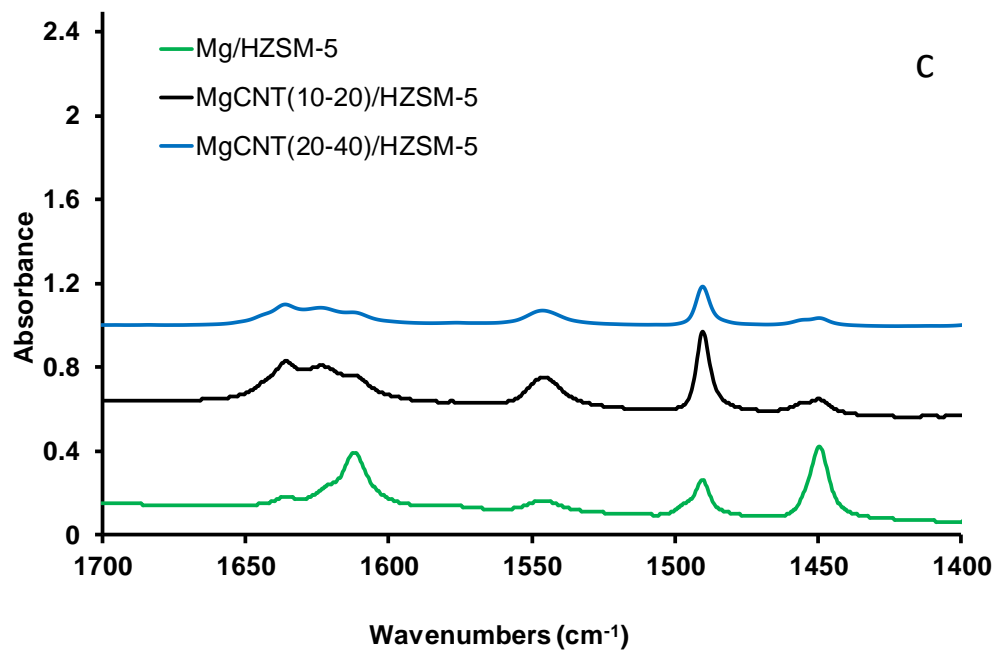


Figure 5. FTIR spectra observed after adsorption of Py on cobalt (a), nickel (b) and magnesium (c) zeolite nanocomposites

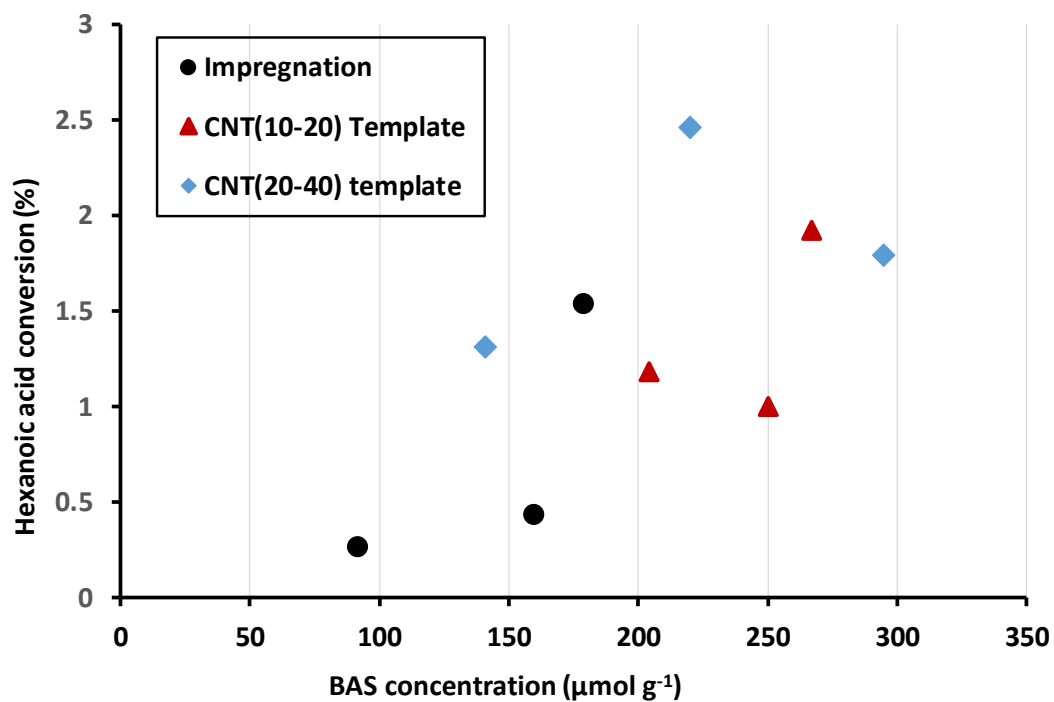


Figure 6. Hexanoic acid conversion in anisole acylation over the metal-zeolite catalysts prepared by impregnation and using Metal/CNT as secondary hard templates.

References

- 1 Corma, A. From Microporous to Mesoporous Molecular Sieve Materials and Their Use in Catalysis, *Chem. Rev.* **1997**, 97, 2373-2419.
- 2 Schüth, F.; Schmidt, W. Microporous and mesoporous materials. *Adv. Mat.* **2002**, 14, 629-638.
- 3 Egeblad, K.; Christensen, C.H.; Kustova, M.; Christensen, C. H. Templating Mesoporous Zeolites, *Chem. Mater.* **2008**, 20, 946–960.
- 4 Ertl, G.; Knözinger, H.; Weitkamp, J. in Preparation of solid acids, Wiley-VCH, Germany 1999.
- 5 Weisz, P.B. Polyfunctional heterogeneous catalysis, *Adv. Catal.* **1962**, 13, 137-190.
- 6 Subramanian, V.; Zholobenko, V.L.; Cheng, K.; Lancelot, C.; Heyte, S.; Thuriot, J.; Paul, S.; Ordonsky, V.V.; Khodakov, A.Y. The Role of Steric Effects and Acidity in the Direct Synthesis of iso- Paraffins from Syngas on Cobalt Zeolite Catalysts, *ChemCatChem* **2016**, 8, 380-389.
- 7 Barrer, R.M. *Hydrothermal Chemistry of Zeolites*. London & New York/Academic Press 1982.
- 8 Ma, Y. ; Tong, W. ; Zhou, H. ; Suib, S.L. A review of zeolite-like porous materials, *Micro and Mesopor. Mat.* **2000**, 37(1-2), 243-252.
- 9 Zečević, J.; Vanbutsele, G.; de Jong, K.P.; Martens, J.A. Nanoscale intimacy in bifunctional catalysts for selective conversion of hydrocarbons, *Nature* **2015**, 528, 247.
- 10 Samad, J. E.; Blanchard, J.; Sayag, C.; Louis, C.; Regalbuto, J.R. The controlled synthesis of metal-acid bifunctional catalysts: The effect of metal:acid ratio and metal-acid proximity in Pt silica-alumina catalysts for n-heptane isomerization, *J. Catal.* **2016**, 342, 203–212.

- 11 Prins, R. Hydrogen Spillover. Facts and Fiction. *Chem. Rev.* **2012**, 112, 2714–2738.
- 12 Im, J.; Shin, H.; Jang, H.; Kim, H.; Choi, M. Maximizing the catalytic function of hydrogen spillover in platinum-encapsulated aluminosilicates with controlled nanostructures, *Nat. Commun.* **2014**, 5, Article number: 3370.
- 13 Tosheva, L.; Valtchev, V.P. Nanozeolites: synthesis, crystallization mechanism, and applications, *Chem. Mater.* **2005**, 17, 2494-2513.
- 14 Jiang, J.; Yu, J.; Corma, A. Extra-large-pore zeolites: bridging the gap between micro and mesoporous structures, *Angew. Chem. Int. Ed.* **2010**, 49, 3120 – 3145.
- 15 Tao, Y.; Kanoh, H.; Abrams, L.; Kaneko, K. Mesopore-modified zeolites: preparation, characterization, and applications, *Chem. Rev.* **2006**, 106, 896-910.
- 16 van Donk, S., Janssen, A.H.; Bitter, J.H.; de Jong, K.P. Generation, characterization, and impact of mesopores in zeolite catalysts, *Catal. Rev. Sci. Eng.* **2003**, 45, 297-319.
- 17 Chen, H.; Wang, Q.; Zhang, X.; Wang, L. Hydroconversion of jatropha oil to alternative fuel over hierarchical ZSM-5. *Ind. Eng. Chem. Res.* **2014**, 53, 19916-19924.
- 18 Schmidt, I.; Boisen, A.; Gustavsson, E.; Ståhl, K.; Pehrson, S.; Dahl, S.; Carlsson, A.; Jacobsen, C. J. H. Carbon Nanotube Templated Growth of Mesoporous Zeolite Single Crystals, *Chem. Mater.* **2001**, 13, 4416-4418.
- 19 Boisen, A.; Schmidt, I.; Carlsson, A.; Dahl, S.; Brorson, M.; Jacobsen, C.J.H. TEM stereo-imaging of mesoporous zeolite single crystals, *Chem. Commun.* **2003**, 958–959.
- 20 Meng, X.; Nawaz, F.; Xiao, F.-C. Templating route for synthesizing mesoporous zeolites with improved catalytic properties, *Nano Today* **2009**, 4, 292-301.
- 21 Zhou, M.; Wang, F.; Xiao, W.; Gao, L.; Xiao, G. The comparison of mesoporous HZSM-5 zeolite catalysts prepared by different mesoporous templates and their catalytic performance in the methanol to aromatics reaction, *Reac Kinet Mech Cat* **2016**, 119, 699–713.

- 22 Sachse, A. ; Wuttke, C. ; Lissner, E. ; Oberson de Souza, M. Ordered Mesoporous ZSM-5 Employing an Imidazolium-Based Ionic Liquid, *Chem. - A Eur. J.* **2014**, 20, 14996–14999.
- 23 Sachse, A. ; Wuttke, C. ; Díaz, U. ; Oberson de Souza, M. Mesoporous Y zeolite through ionic liquid based surfactant templating, *Micro Mesopor Mater.* **2015**, 217, 81–86.
- 24 Zhai, Y.; Zhu, Z.; Dong, S. Carbon-based nanostructures for advanced catalysis, *ChemCatChem* **2015**, 7, 2806-2815.
- 25 Liu, W.-W.; Chai, S.-P.; Mohamed, A.R.; Hashim, U. Synthesis and characterization of graphene and carbon nanotubes: A review on the past and recent developments. *J. Ind. Eng. Chem.* **2014**, 20, 1171-1185.
- 26 Diehl, F. ; Khodakov, A.Y. ; Promotion of cobalt Fischer-Tropsch catalysts with noble metals: A review, *Oil and Gas Science and Technology* **2009**, 64, pp.11-24.
- 27 Flores, C.; Batalha, N.; Ordonsky, V.; Zholobenko, V.L.; Baaziz, W.; Marcilio, N.R.; Khodakov, A.Y. Direct production of iso-paraffins from syngas over hierarchical cobalt-ZSM-5 nanocomposites synthesized by using carbon nanotubes as sacrificial templates, *ChemCatChem*, **2018**, 10, 2291-2299.
- 28 Peron, D. V. : Zholobenko V. L. ; Rodrigues de la Rocha, M. ; Oberson de Souza, M. ; Feris, L. A. ; Marcilio, N. R. ; Ordonsky, V. V., Khodakov, A. Y. Nickel–zeolite composite catalysts with metal nanoparticles selectively encapsulated in the zeolite micropores. *J. Mat. Sci.*, **2019**, 54, 5399-5411.
- 29 van't Blik, H.F.J.; Prins, R. Characterization of supported cobalt and cobalt-rhodium catalysts: III. Temperature-Programmed Reduction (TPR), Oxidation (TPO), and EXAFS of Co-Rh/SiO₂. *J. Catal.* **1986**, 97, 210-218.

- 30 Hong, J.; Marceau, E.; Khodakov, A.Y.; Griboval-Constant, A.; La Fontaine, C.; Villain, F.; Briois, V.; Chernavskii, P.A. Impact of sorbitol addition on the structure and performance of silica-supported cobalt catalysts for Fischer–Tropsch synthesis, *Catal. Today* **2011**, 175, 528-533.
- 31 Khodakov, A.Y.; Griboval-Constant, A.; Bechara, R.; Villain, F. Pore-size control of cobalt dispersion and reducibility in mesoporous silicas, *J. Phys. Chem. B* **2001**, 105, 9805-9811.
- 32 Carvalho, A.; Marinova, M. ; Batalha, N. ; Marcilio, N.R. Khodakov, A.Y.; Ordonsky, V.V. Design of nanocomposites with cobalt encapsulated in the zeolite micropores for selective synthesis of isoparaffins in Fischer–Tropsch reaction, *Catal. Sci. Technol.* **2017**, 7, 5019-5027.
- 33 Stakheev, A.Y.; Khodakov, A.Y.; Kustov, L.M.; Kazansky, V.B.; Minachev, K.M. Localization of polyvalent cations in pentasil catalysts modified by metal oxides. *Zeolites* **1992**, 12, 866-869.
- 34 Khodakov, A.Y.; Lynch, J.; Bazin, D.; Rebours, B.; Zanier, N.; Moisson, B.; Chaumette, P. Reducibility of cobalt species in silica-supported Fischer–Tropsch catalysts, *J. Catal.* **1997**, 168, 16-25.
- 35 Puskas, I.; Meyers, B. L.; Hall, J. B. Activity decline and diffusional changes in a magnesium-promoted cobalt-silica catalyst, *Catal. Today* **1994**, 21, 243–251.
- 36 Jong, S.-J.; Cheng, S. Reduction behavior and catalytic properties of cobalt containing ZSM-5 zeolites, *Appl. Catal. A* **1995**, 126, 51–66.
- 37 Tomiyama, S.; Takahashi, R.; Sato, S.; Sodesawa, T.; Yoshida, S. Preparation of Ni/SiO₂ catalyst with high thermal stability for CO₂-reforming of CH₄. *Appl. Catal. A* **2003**, 241, 349-361.

- 38 Soghrati, E., Kay, T.; Ong, C.; Kok Poh, C.; Kawi, S.; Borgna, A. Zeolite-supported nickel phyllosilicate catalyst for CO hydrogenolysis of cyclic ethers and polyols, *Appl. Catal. B* **2018**, 235, 130-142.
- 39 Maia, A.J.; Louis, B.; Lam, Y.L.; Pereira, M.M. Ni-ZSM-5 catalysts: Detailed characterization of metal sites for proper catalyst design, *J. Catal.* **2010**, 269, 103–109.
- 40 Romero, M.D.; de Lucas, A.; Calles, J.A.; Rodriguez, A. Bifunctional catalyst Ni/HZSM-5: effects of the nickel incorporation method, *Appl. Catal. A* **1996**, 146, 425-441.
- 41 Chen, B.-H.; Chao, Z.-S.; He, H.; Huang, C.; Liu, Y.-J.; Yi, W.-J.; Wei, X.-L.; An, J.-F. Towards a full understanding of the nature of Ni(ii) species and hydroxyl groups over highly siliceous HZSM-5 zeolite supported nickel catalysts prepared by a deposition-precipitation method. *Dalton Trans.* **2016**, 45, 2720-2739.
- 42 Chen, B.-H.; Liu, W.; Li, A.; Liu, Y.-J.; Chao Z.-S. A simple and convenient approach for preparing core-shell-like silica@ nickel species nanoparticles: highly efficient and stable catalyst for the dehydrogenation of 1, 2-cyclohexanediol to catechol, *Dalton Trans.* **2015**, 44, 1023-1038.
- 43 Iglesia, E.; Reyes, S.C.; Madon, R. J. and Soled, S.L. Selectivity Control and Catalyst Design in the Fischer-Tropsch Synthesis: Sites, Pellets, and Reactors, *Adv. Catal.* **1993**, 39, 221-302.